Report for Austrian Marshall Plan Foundation

Novel materials with potential for interesting light-dependent, energy conversion capabilities. Growth, structural characterization and investigation of thin film properties

THOMAS MÖSL

Department of Materials Science and Engineering
University of California, Berkeley
April 3, 2015 to Sep. 1, 2015

Supervisor:

Associate Professor Lane Wyatt Martin

Graz, January 30, 2016

ACKNOWLEDGEMENTS

First of all, I want to give a special thanks to my supervisor Associate Professor **Martin Lane** for giving me the opportunity to be part of his research group at the University of California, Berkeley, Department of Materials Science and Engineering. I am grateful for his extraordinary support and assistance during my time in Berkeley.
The collaborative work in the research lab during my time, was one of the most rewarding experience. Furthermore, I want to acknowledge the efforts of all members of his research group for assisting me with the PLD setup, measurement and understanding.

Discussions about my research topic, assistance and advice throughout this project made it possible to complete my tasks successfully and expand my knowledge in the fascinating world of multifunctional materials and their physical behavior. Last, I want to credit the following individuals for their time and for their exceptional help regarding:

Concept of pulsed laser deposition

Anoop Damodaran, Ran Gao, Claudy Rayan Serrao and Ajay Yadav

Structural characterization and data analysis

Ran Gao, Shishir Pandya,James Clarkson, Brent A. Agpar, Josh Agar and Liv Dedon

Fabrication processes such as photolithography, sputter deposition etc.

Shishir Pandya, Sahar Saremi and Brent A. Agpar

This internship was made possible by the **Marshall Plan Scholarship**. I appreciate the Austrian Marshall Plan Foundation for providing financial support, which enabled me to be part of the research group and to work on a state-of-art research topic.

Contents

List of Figures

List of Symbols and Abbreviations

PVO - Lead vanadate, $PbVO_3$

MRD - Materials research diffractometer

HRXRD - High resolution X-ray diffractometry

RSM - Reciprocal space mapping

UHV - Ultra high vacuum

XRR - X-ray reflectivity

SPM - Scanning probe microscopy

AFM - Atomic force microscopy

PFM - Piezoresponse force microscopy

PSD - Position sensitive detector

VdW - Van Der Waals forces

PEM - Photoelastic modulator

LAO - Lanthanum aluminate, $LaAlO_3$

STO - Strontium titanate, $SrTiO_3$

LSAT - Lanthanum aluminate-strontium aluminium tantalate, $(La_{0.18}Sr_{0.82})(Al_{0.59}Ta_{0.41})$

BFO - Bismuth ferrite, $BiFeO_3$

PLD - Pulsed laser deposition

IPA - Isopropyl-alcohol

FWHM - Full-width-at-half-maximum

Pt - Platinum

ITO - Indium tin oxide

SnO_2 - Tin (IV) oxide

In_2O_3 - Indium (III) oxide

RMS - Rout mean square

RBS - Rutherford backscattering spectrometry

SVO - Strontium vanadate, $SrVO_3$

SRO - Strontium ruthenate, $SrRuO_3$

LNO - Lanthanum nickelate, $LaNiO_3$

PTO - Lead titanate, $PbTiO_3$

PR - Photoresist

UV - Ultraviolet

E_g - Semiconductor band gap

1 Introduction

I am Thomas Moesl, and I have been studying Technical Physics at the Graz University of Technology since 2009. For my bachelor thesis I worked in a laboratory at the Max Plank Institute of Quantum Optics in Munich. Currently I am completing my Master's degree Advanced Materials Science with an emphasis on Semiconductor Processing and Nanotechnology. After my internship in Munich, I was looking for another opportunity to research in a state-of-the-art facility while studying abroad, which inspired me to apply for an internship in the USA. With the help and trust of Associate Prof. Martin Lane and financial support by the Marshall Plan foundation, I was able to be a part of his research group in the Department of Materials Science and Engineering at the University of California Berkeley from April 3, 2015 to September 1, 2015.

My project was to research novel materials that have the potential for interesting light-dependent, energy conversion capabilities. Based on prior work by Associate Prof. Martin Lane and his research group, I investigated the newly discovered polar material, $PbVO_3$. I synthesized this material as single layer on a substrate and subsequently characterized the structure. Next, I produced a device of layered structures to investigate the properties of $PbVO_3$ in dark and light conditions. The characterization was done using X-ray diffraction, scanning probe microscopy (atomic force microscopy, piezoresponse force microscopy), and probe station for dielectric/electrical studies.

This report summaries up my work in the Department of Materials Science and Engineering at the University of California, Berkeley. It includes information about the material, ways to synthesize layered structures (devices), methods to characterize the materials and data analysis. This report shows foundational materials science knowledge including aspects of materials synthesis, characterization and fabrication.

2 General Background

In recent years, multiferroic materials in which magnetism and ferroelectricity coexist have become the focus of attention in Materials Science due to their technological and fundamental significance. [1, 2, 3, 4] The challenge to synthesize novel materials and to characterize their structure and properties has attracted significant research interest worldwide [5, 6]. This leads to a broad variety of high tech functional devices based on thin films. For a proper investigation of new materials, especially thin films, the following analyzing methods were used during my internship at the University of California, Berkeley.

2.1 Investigation and Characterization Methods

2.1.1 High Resolution X-Ray Diffractometry (HRXRD)

High Resolution X-Ray Diffractometry is one of the most popular methods to determine the crystal structure of a material. It is possible to control the analysis depth by the incident angle onto the surface and to investigate buried interface structure, which is very essential for thin films. Based on the operation mode, one can verify if the film has a large anisotropy either along the out-of-plane axis (thickness) or in the in-plane axis (within surface plane) [7]. A large anisotropy can have a significant influence on physical properties of thin films. Therefore a detailed analysis of the structural and textural properties with proper X-ray optics was necessary [8].

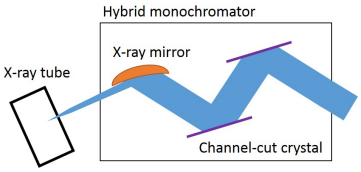

Figure 1: Schematic illustration of the beam path through the PreFIX 2-bounce hybrid monochromator [9].

All the HRXRD measurements were performed with the X'Pert Materials Research Diffractometer (MRD) system by *PANalytical*.
The centerpiece is PreFIX 4-bounce hybrid monochromator, which consisted of an X-ray mirror and a channel-cut-germanium crystal. The mirror collimates the divergent beam from the line of Cu_{α_1} X-ray tube to a parallel beam. Using a 4 bounce channel-cut Ge crystal, a high intensity and resolution monochromatic

parallel beam was created. **Figure 1** shows a sketch of the beam path through the optical setup. The difference is only the number of reflections (two or four) in the channel-cut crystal.

Table 1: Characterization methods of thin films [7].

Method	Obtainable information
Out-of-plan measurement	Phase identification, crystal structure
In-plane measurement	Phase identification, crystal structure
Reciprocal space maping (RSM)	Crystrallinity, distortion/relaxation of the film
Phi-scan	Epitaxy
X-ray reflectivity measurement (XRR)	Film thickness, density and roughness

2.1.2 Scanning Probe Microscopy (SPM)

SPM is a branch of microscopy that provides images of surface topography and properties on an atomic scale [10]. **Figure 2** illustrates a simple SPM setup. The probe tip was mounted at the end of the cantilever which was attached to a piezo tube scanner.

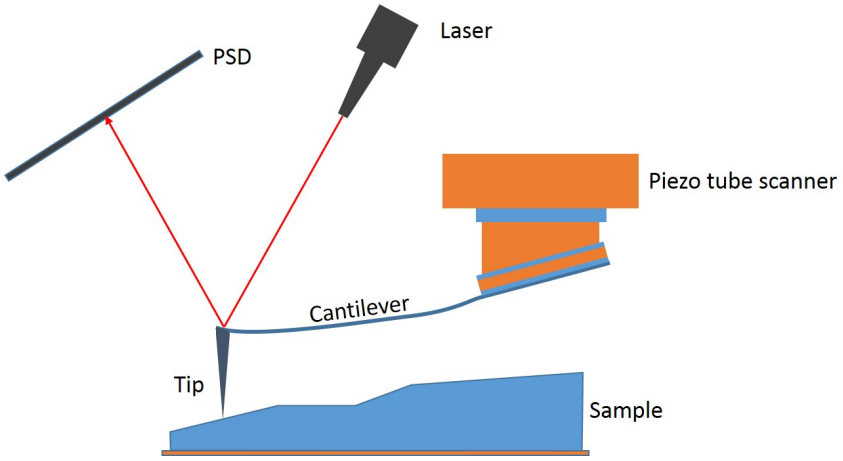

Figure 2: Primary setup of SPM including tip, cantilever, piezo tube scanner, the laser and the position sensitive detector

The probe tip scans the sample back and forth. Due to interactions between the probe tip and the sample's surface, the cantilever becomes deflected. This change in height was measured by the laser that was reflected off the top of the cantilever into a Position Sensitive Detector (PSD). Using the electronic feedback, the measured deflection of the cantilever creates an image. The force on the tip was controlled by the piezo element and monitored via the PSD.

According to the effective force that causes the interaction, there are different types of scanning probe microscopes [11, 12]. For this, we used an atomic force microscope (AFM) and a piezoresponse force microscope (PFM).

- AFM

  The most common modes are contact and tapping mode. In the contact mode, it is possible to have a constant deflection due to the force control via the movement of the piezo-element in z-direction (constant PSD position = constant force). For tapping mode, the amplitude is kept constant (= constant force) by the piezo-element [13]. Depending on the distance between the tip and the surface, the interaction between them changes. **Table 2** gives an overview of sample interactions.

Table 2: Tip - sample interactions
a, b and c represent constants.

Distance r	Interaction	Potential
>10 nm	electrostactic, magnetic	$\frac{c}{r^2}$
10 nm to 0.5 nm	Van Der Waals forces (VdW)	$-\frac{b}{r^6}$
<0.2 nm	electron-electron repulsion	$\frac{a}{r^{12}}$

- PFM

  This type of SPM is focused on imaging and manipulating of ferroelectric domains. Ferroelectric materials, which posses a permanet dipol and a spontaneously reversible electric polarization, are a unique among the piezoelectrics. By applying mechanical stress to a piezoelectric material, surface charges or polarization accumulates. The reverse piezoelectric effect describes the deformation of the material by applying an electric field [13]. Therefore, it is possible to permanently switch between two different states "1" and "0" [15]. This is achieved by applying an AC voltage to a conducting tip as a movable top electrode coupled to the ferroelectric surface.

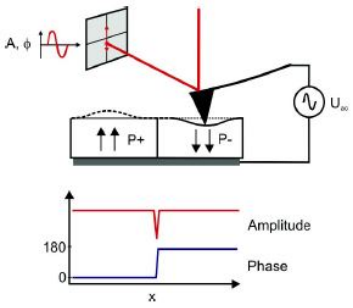

Figure 3: Sketch of a regular PFM.Top: AC voltage is applied between the tip and sample. Bottom: Phase and voltage change based on the domain orientation vs. the bias sign [14].

  Depending on the alignment of the applied electric field and the polarization, the sample locally expanded (in-phase response $P+$) or contracted (out-of-phase response $P-$), which results in a phase and amplitude change as illustrated in **Figure 3** [14].

2.1.3 Probe Station

The investigation of electrical and dielectric properties of a single layer or device composed of novel materials was achieved by the probe station.

Micromanipulators with specific probe tips were precisely placed on the surface of the device (2 point method). By applying a voltage, the electrical behavior was measured and visualized using software by *Radiant Technologies*. For my project, we focused on the measurement of I-V curves in dark and light conditions, polarization, capacitance, resistance and dielectric constant.

2.1.4 Ellipsometry

An ellipsometry consists of a light source, polarizer, compensator, analyzer and detector which is schematically shown in **Figure 4**. Using an optional photoelastic modulator (PEM), it was possible to modulate the polarization of the incoming light beam. PEM measures the change in polarization which was quantified by the amplitude ratio Ψ and the phase difference Δ upon reflection. Both are related to the ratio of Fresnel complex reflection coefficients for parallel and perpendicular polarized light referring to the plane of incidence. Due to the fact that this measurement is an indirect method, a model analysis was necessary to obtain the optical constants (dielectric properties) and thickness of the sample. In the following equation, ρ defines the complex reflectance ratio.

$$\rho = \frac{r_p}{r_s} = tan(\Psi) \cdot e^{i\Delta} \tag{2.1}$$

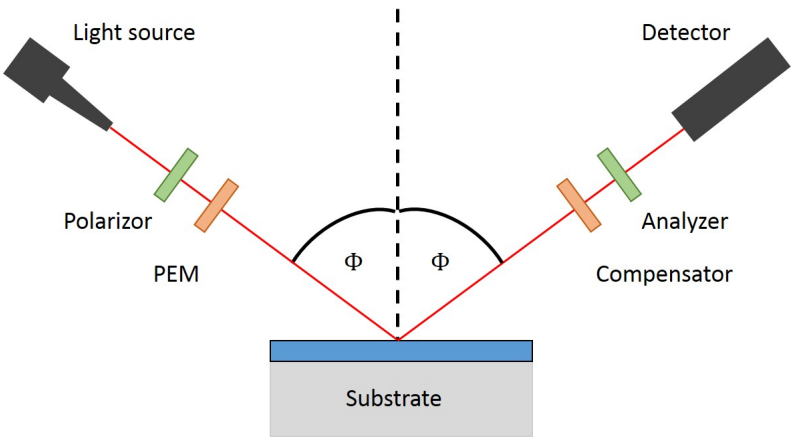

Figure 4: Illustration of an ellipsometry setup. The angle Φ of the incidence equals the angle of reflection. Ellipsometry belongs to specular optical techniques.

3 Experimental Section

This chapter begins with a brief introduction of the novel material lead vanadate (PVO), strontium vanadate (SVO), and the substrate lanthanum aluminate (LAO), including the latest results by different research groups. This chapter focuses on growth techniques of novel materials, characterization of their structure, investigation of their properties, and data analysis.

3.1 Introduction to $PbVO_3$, $LaAlO_3$ and $SrVO_3$

3.1.1 Lead vanadate ($PbVO_3$)

In the search for novel single phase multiferroic materials, lead vanadate ($PbVO_3$) was among possible candidates [6]. PVO, as part of the perovskite oxide family, has attracted significant research interest in hope to gain a single phase multiferroic with strong coupling between ferroelectric and magnetic order parameters at room temperature [2].

Figure 5b illustrates the ideal structure of cubic ABX_3 perovskite. It consists of corner sharing $[BX_6]$ octahedra with the A cation occupying the 12-fold coordination site in the middle of the cube [16]. Due to size effects, deviation from the ideal composition, and the Jahn-Teller effect, most of the perovskite systems are distorted which is important for their magnetic and electrical properties.

At this point, single phase multiferroic has been found in only a few perovskite oxides. The most studied of which is the antiferromagnetic, ferroelectric $BiFeO_3$. The lone pair of the large A-site ion creates the ferroelectric properties, whereas the smaller B-site ions provide the magnetic properties [17, 18]. PVO belongs to the ABO_3 perovskites and is based on the same principle as $BiFeO_3$. The stereochemical activity of the 6s lone pair of Pb creates ferroelectricity and the d^1 electric configuration on the vanadium ion controls the magnetic properties.

Initial results of bulk PVO, synthesized under high pressure and high temperature, revealed the highly tetragonal distorted perovskite structure with space group P4mm. The corresponding lattice parameters are a = 3.79995(8) Å and c = 4.6704(2) Å (c/a = 1.23) and a = 3.80391(5) Å and c = 4.67680(8) Å (c/a = 1.23) [19, 20].

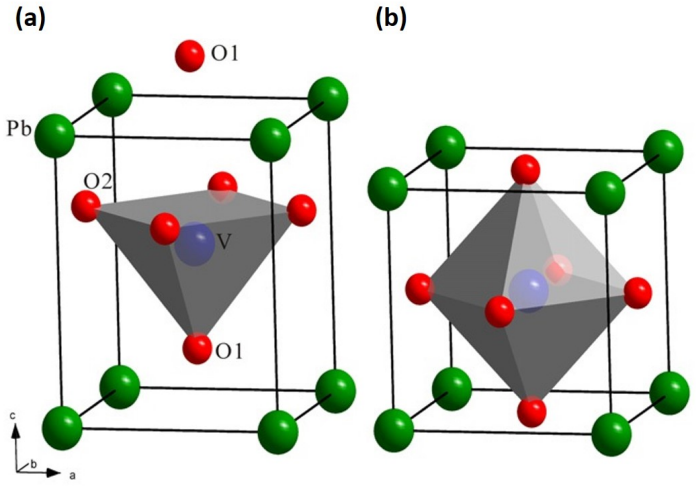

Figure 5: Crystal structure of $PbVO_3$ perovskites. (a) Tetragonal phase (P4mm) shows the shift of the central V atom (V^{4+}-ion). The distortion induces one of the two apical oxygen atoms (O1) to seperate from the octahedron, forming corner shared square pyramids VO_5 [6]. (b) Cubic phase ($Pm\bar{3}m$) with the central V atom arranged in a octahedral configuration VO_6.

Due to the strong tetragonal distortion (**Figure 5a**), isolated layers of corner-shared VO_5 pyramids were formed instead of the octaheadra [19].

Furthermore, PVO has been proposed to have antiferromagntic ordering and a ferroeletric polarization of 152 µC/cm caused by the high tetragonal distortion [21, 19, 20]. The P-E hysteresis of polarization was not observed in PVO due to the large distortion and low resistivity [22, 23].

By using pulsed laser deposition (PLD) thin films of PVO were synthesized on $LaAlO_3$ (001) in reducing environments (10^{-6} to 10^{-5} torr) at temperatures ranging from 450 to 650 °C [2, 24]. Furthermore, it was possible to stabilize PVO in a greater tetragonally distorted pervoskite structure (a = 3.79 Å and c = 5.02(2) Å (c/a = 1.32)).
Studies have shown that PVO thin films are piezoelectric at room temperature (piezoelectric coefficient d_{33} of about 3.1 pC/N) and exhibit a G-type antiferromagnetic order below 130 K [24].

In summary, lead vanadate ($PbVO_3$) is indeed a multifunctional material, but is not multiferroic. It is polar and piezoelectric, but the extreme tetragonal distortion prevents the material from being ferroelectric. Between 100 to 130 K, PVO undergoes a magnetic phase transition. This low temperature phase of PVO is likely to be both polar, piezoelectric and G-type antiferromagnet [24].

3.1.2 Lanthanum Aluminate ($LaAlO_3$)

For my project, I only used substrates from the company *CrysTec*, including strontium titanate (STO) (001), lanthanum aluminate - strontium aluminium tantalate (LSAT) (001) and lanthanum aluminate (LAO) (001)(**Table 3**). Based on the revealed in-plane lattice parameter a = 3.80391(5) Å of bulk PVO, LAO had the best lattice match (in-plane) for the subsequent growth to become fully strained epitaxial thin films of PVO on LAO (001) [20]. Due to failed initial attemps, I only focused on LAO (001) substrates, to achieve fully strained epitaxial thin films of PVO.

Lanthanum aluminate (LAO) structure is a rhombohedral distorted perovskite with a pseudocubic lattice, including micro twins parallel (100). The lattice parameter is a = 3.79 Å at room temperature.

Table 3: Overview of substrates and their lattice parameters

Substrate	Crystal structure	a (Å)	Orientation
LAO	pseudocubic, micro twins parallel (100)	3.799	(001)
STO	pseudocubic, twin free	3.905	(001)
LSAT	pseudocubic, twin free	3.868	(001)

3.1.3 Strontium Vanadate ($SrVO_3$)

SVO has a cubic perovskite structure (**Figure 6**) with a lattice constant of a = 3.8425(1) Å, space group $Pm\bar{3}m$ [25]. In contrast to PVO, the central atom (V^{4+}-ion) is not shifted, hence there is no ferroelectric instability [26]. It has been reported that strontium vanadate is an n-type metallic conductive oxide.

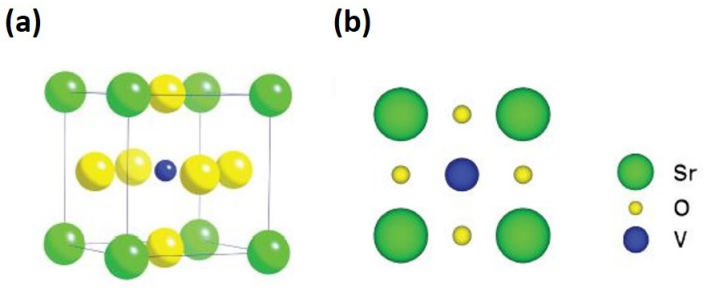

Figure 6: Crystal structure of $SrVO_3$ perovskites. (a) Cubic perovskite structure $Pm\bar{3}m$ at room temperature. Central V atom arranged in a octahedral configuration VO_6 (b) [100] view of SVO [27].

Based on the low resistivity, atomically smooth surface and excellent structural and chemical compatibility, $SrVO_3$ is considered to be one of the best materials for applications such as electrodes [25, 28].

3.2 Preparation and Maintenance of the PLD Setup

All thin films studied in this report were synthesized by using pulsed laser deposition (PLD). A more detailed description and illustration of the PLD setup is provided in the Appendix.

Preparation and maintenance of the chamber and substrates are necessary in order to obtain high quality films without contaminations. Therefore, it is important to note that:

- All substrates were ultrasonicated in acteone for 5 minutes to remove any contamination, followed by an ultrasonic bath in isopropyl−alcohol (IPA) for 5 minutes to remove any traces of acetone.
- UHV chamber was cleaned with IPA and *Kimwipes* to get rid of residues of previous depositions
- Heater surface was sanded (sandpaper 600-Grit) and wiped with IPA
- Entrance window for the laser beam was cleaned with 0.05 µm colloidal silica suspension followed by IPA
- Target was sanded and blown with air to ensure a plane and not contaminated surface, followed by 4 minutes of pre-ablation under growth conditions prior PLD

Substrates were adhered to the substrate heater using silver ink (*Leitsilver 200, Ted Pella, Inc.*) It was important to align the substrates with target position, to ensure that the plasma plume was focused on the substrate during the deposition. The geometric arrangement is illustrated in **Figure 20**

In order to achieve an effective vacuum, initially a rotary vane pump (*DUO 20M, Peiffer vacuum*) was used to reach a base pressure of 3×10^{-2} torr. Then a turbomolecular pump (*TMU 261 Y P, Pfeiffer vacuum*) was necessary to establish the final pressure of ($\sim 10^{-8}$ torr). Laser energies were measured by a *Gentec−eo* pyroelectric laser power and energy meter. Thermal paper was used to obtain the spot size, which was needed to calculate the laser fluence. The alignment of the optical setup was found by using thermal paper and the energy meter. After the completion of the thin film deposition, substrates were cooled down under deposition conditions.

3.3 Growth and Structure of $PbVO_3$ Thin Films

Laser Parameters

All thin films were grown from a target with stoichiometry $PbVO_3$ using a KrF excimer laser (*Lambda Physik Lextra*) with wavelength 248 nm. The laser operated at a repetition rate of 10 Hz with a laser fluence of $0.70 \pm 0.03\,J/cm^2$.

Deposition Parameters

The deposition of PVO took place under 100 mtorr of inert gas Argon at temperatures ranging from 530 to 570 °C. Under these conditions thin films of PVO with a thickness of 150 to 220 nm were grown on the substrate $LaAlO_3$ (LAO) (001).

3.3.1 Characterization Results

The structure analysis of PVO thin films (150 to 220 nm) on LAO (001) substrates was done using X-ray diffraction (X'Pert Materials Research Diffractometer (MRD) system by *PANalytical*). More information about X-ray diffraction is given in section 2.1.1. **Figure 7a** confirms that all films were (00l) oriented and single phase. There were no secondary phases present. The PVO 002 peak full-width-at-half-maximum (FWHM = 0.13686)° showed us that all films are highly crystalline and ordered. Based on the $2\Theta/\Theta$-scan, the out-of-plane, c-lattice parameter of the distorted perovskite structure of PVO was determined to be 5.02 Å, in agreement with literature [2]. The exact calculation can be found in section 6.3. **Figure 7b** shows the in-plane epitaxial relationship between the film (f) and substrate (s). All films were fully epitaxy with $(011)_f||(011)_s$. Phi-scans revealed the in-plane a-lattice parameter to be 3.79 Å, in agreement with literature [2].

Reciprocal space maps in the vicinity of $(\bar{1}03)$ were collected. **Figure 8c** shows that all films were fully strained on LAO (001). The PVO lattice was constrained to the LAO substrate lattice so that the reciprocal lattice points were lined in the vertical direction. The distance between PVO $\bar{1}03$ and LAO $\bar{1}03$ diffraction peak confirmed the big tetragonal distortion. These lattices had the same length in the horizontal direction. Thereof, the c-lattice parameter was determined. Further information about epitaxial and fully strained films is given in the Appendix. In summary, (00l) oriented, single phase, fully epitaxial and strained thin films of PVO were grown on LAO (001) using PLD.

The investigation of the surface morphology was done by the AFM. Further information about AFM can be found in section 2.1.2. The results are shown in **Figure 9**. The relatively rough thin film morphology (**Figure 9b**) corresponds to a average rout mean square (RMS) roughness of 9 nm.

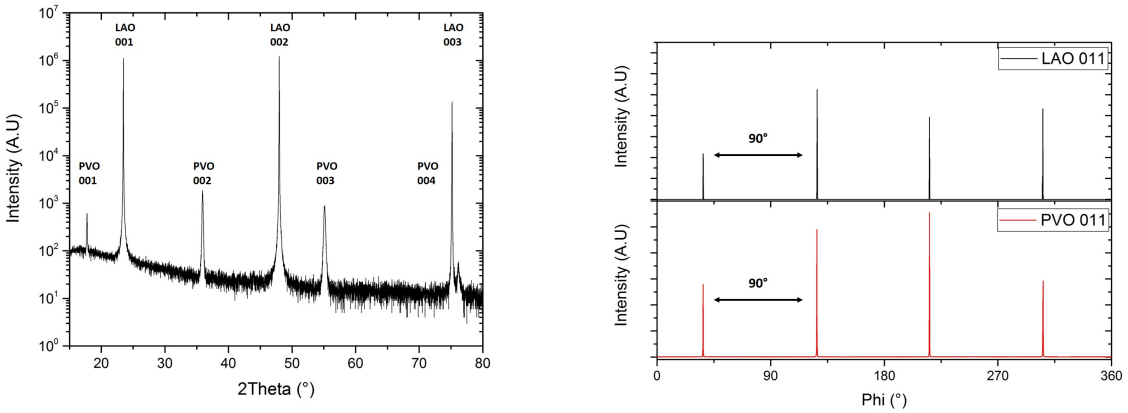

(a) (b)

Figure 7: $PbVO_3$ thin films on $LaAlO_3$ (001) substrate. Structural characterization by using X-ray diffraction (a) $2\Theta/\Theta$-scan displays a single phase, highly crystalline thin film. (b) Phi-scans of PVO and LAO shows the in-plane expitaxial relationship $(011)_f||(011)_s$ and revealed the in-plane a-lattice parameter to be 3.79 Å.

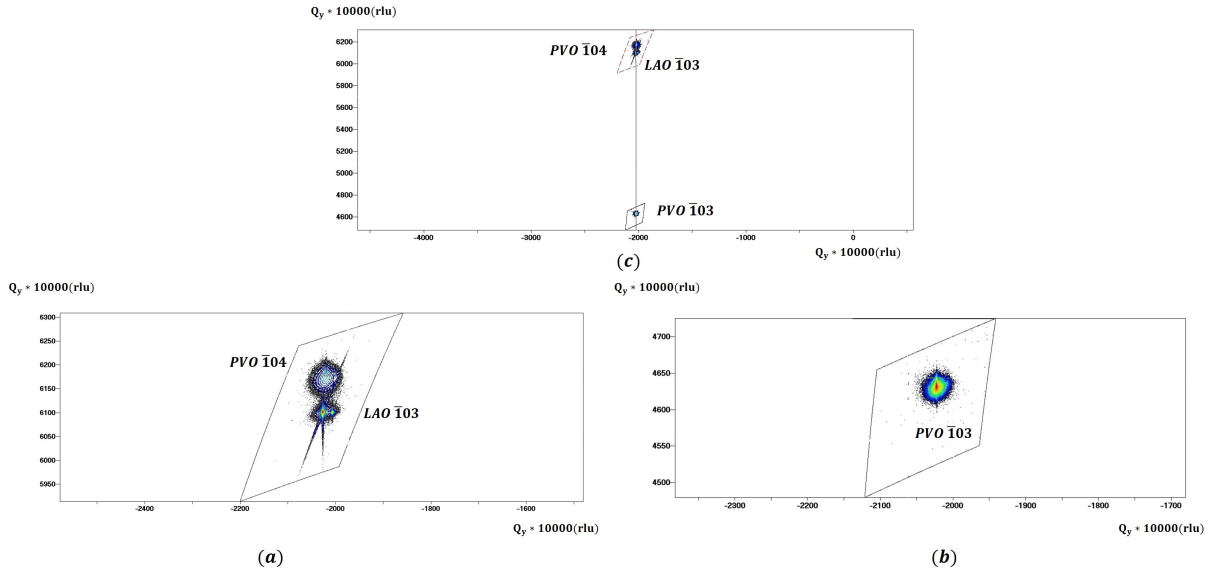

Figure 8: Schematic illustration of RSM results of PVO on LAO (001) in the vicinity of $\bar{1}03$ diffraction peak. (a) Due to the high tetragonal distortion, the diffraction peak $\bar{1}04$ of PVO got collected as well. Micro twins of LAO parallel to (100) can be seen next to the LAO $\bar{1}03$ peak. (b) shows the diffraction peak PVO $\bar{1}03$ and (c) revealed the highly tetragonal distortion and and confirmed that all PVO films are fully strained

Data analysis was done using the software *NanoScope Analysis 1.5, Bruker*. Due to the relatively rough surface, thickness was determined by using rutherford backscattering spectrometry (RBS) instead of XRR.

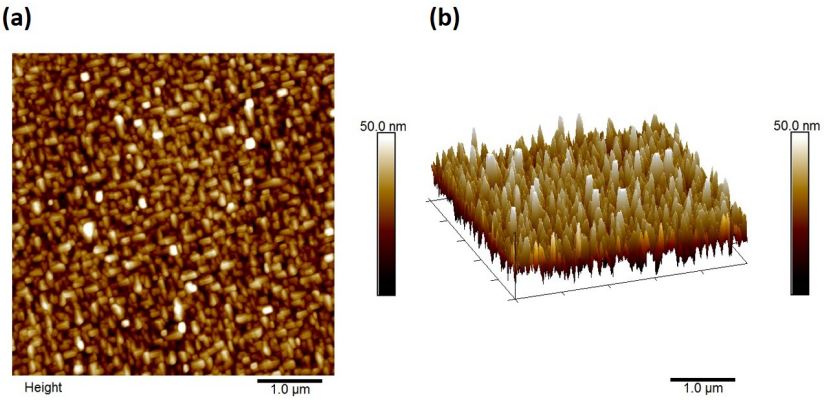

Figure 9: Surface morphology of PVO thin films using AFM, (a) 2D image (b) 3D image. All films showed a RMS roughness on the order of ∼9 nm.

3.4 Growth And Structure of $SrVO_3$ Thin Films

On the side, I synthesized strontium vanadate ($SrVO_3$) on LAO (001) using the same PLD system. The goal was to find an appropriate electrode for the PVO device building process and upcoming electrical and dielectric measurements.

Laser Parameters

All SVO thin films were grown from a target with stoichiometry $SrVO_3$ using a KrF excimer laser (*Lambda Physik Lextra*) with wavelength 248 nm. The laser operated at a repetition rate of 1 Hz with a laser fluence of $1.12 \pm 0.03\,\mathrm{J/cm^2}$.

Deposition Parameters

Growth of SVO occurred under 10 mtorr of inert gas Argon at 700 °C. Thin films of SVO with a thickness of 10 to 75 nm were grown on the substrate $LaAlO_3$ (LAO) (001).

3.4.1 Characterization Results

Structural characterization was done using X-ray diffraction. The results are shown in **Figure 10a**. $2\Theta/\Theta$-scan revealed the high crystallinity and single phase of $SrVO_3$ on LAO (001). Additionally X-ray reflectivity measurements (XRR) were performed to obtain more information about the material **(Figure 10b)**. By using the *PANalytical* Reflectivity software, the results were evaluated and the layer thickness was determined.

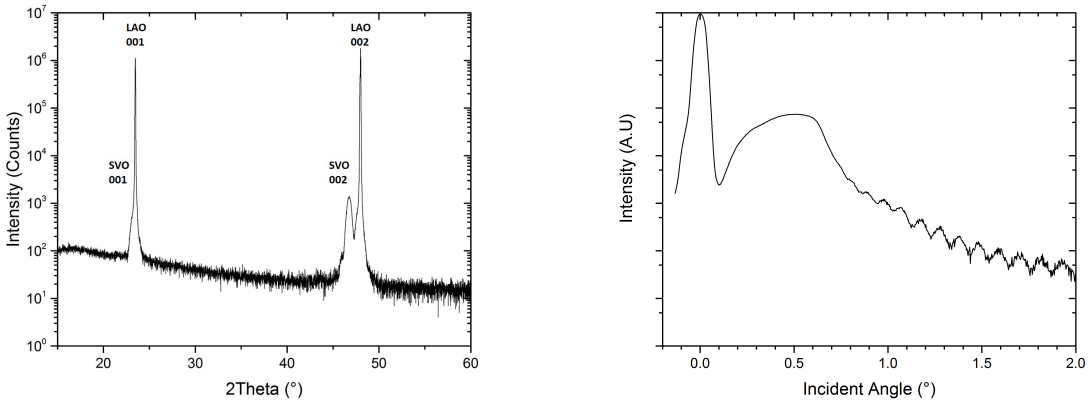

(a) (b)

Figure 10: Structural characterization of $SrVO_3$ thin films on $LaAlO_3$ (001) substrate. (a) $2\Theta/\Theta$-scan shows highly crystalline and single phase films on LAO (001). (b) X-ray reflectivity was used to determine the thickness of the SVO film. For this film the average thickness was 74 nm.

The fitting parameter for this specific XRR can be found in the Appendix. As mentioned in 3.1.3, SVO is considered to be one of the best materials for applications as electrodes. The roughness of the materials is critical for establishing a good interface between them. All SVO thin films on LAO (001) showed smooth surface morphologies (RMS roughness on the order of ∼0.32 nm) in comparison to PVO (**Figure10**).

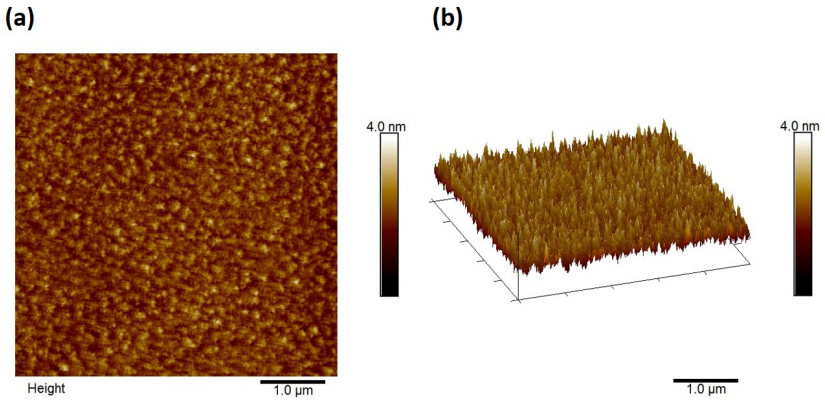

Figure 11: Surface morphology of SVO thin films using AFM, (a) 2D image (b) 3D image. All films showed a RMS roughness on the order of ∼0.32 nm.

3.5 Growth of ITO Using PLD

In addition, I synthesized indium tin oxide (ITO) on top of the PVO films using the same PLD system. It is one of the most widely used transparent conducting oxides, because of a tunable work function, high visible light transmittance, low resistivity and excellent adhesion to substrates [29, 30]. There is always a trade-off between the transmittance and conductivity. Post annealing (**Figure 12**) is used to enhance or adjust optical transmittance and electrical resistivity [31]. Furthermore, it is a heavily doped n-type semiconductor with a wide band gap $\sim$4 eV [32].

Laser Parameters

All ITO layers were grown from a target with composition of 10 % SnO_2 and 90 % In_2O_3. The same PLD system inclusive the laser was used for all depositions. The laser operated at a repetition rate of 5 Hz with a laser fluence of $1.16 \pm 0.03\,\mathrm{J/cm^2}$.

Deposition Parameters

Growth of ITO took place in 20 mtorr of oxygen (O_2) at room temperature. Thin films of ITO with a thickness of 100 nm were grown on top of PVO films. Here, the substrate was adhered on the substrate heater with carbotape.

Post Annealing

Figure 12 shows the temperature ramp to enhance optical transmittance and electrical resistivity. X-ray diffraction revealed that the post annealing process (holding the sample at 300 °C for 30 minutes) had no influence on the PVO film. Therefore, it was possible to use ITO as a top electrode for optical measurements.

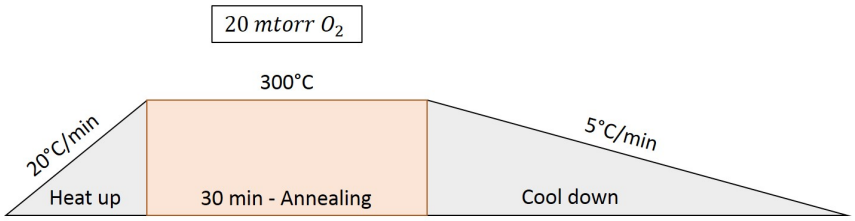

Figure 12: Temperature ramp for the post annealing process of indium tin oxide (ITO). The thin layer is hold at 300 °C for 30 minutes.

3.6 Synthesis of Layered Structures by PLD

In this section, I introduce design algorithms for the creation of electronic device structures, including materials like platinum (Pt) and indium tin oxide (ITO). Sputter deposition and photolithography are introduced as important steps on the way to the final device as well.

3.6.1 Device Structures

There are many device structures (electrode geometries) that are used for a broad range of different measurements for specific properties of multifunctional materials. In this project, I focused on in-plane and out-of-plan electrical and dielectric measurements. The pattern for both electrode geometries can be fabricated with the etch or lift-off process. Due to few results using the etch process, all geometries were developed by using photolithography in combination with the lift-off process. A more accurate description of photolithography can be found in the Appendix.

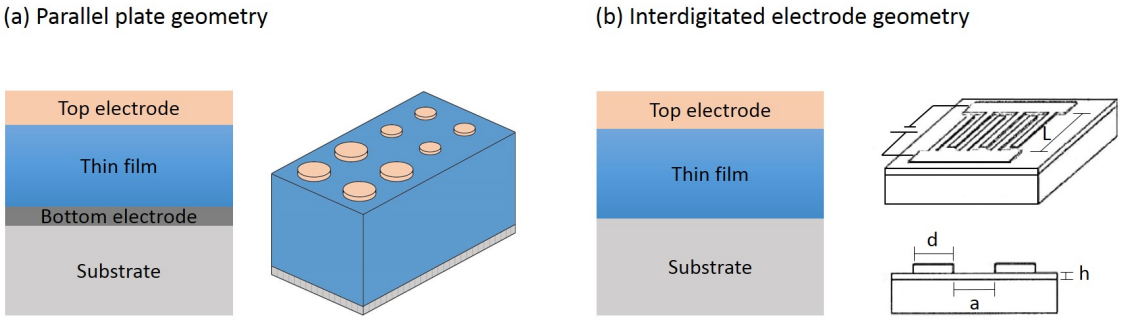

Figure 13: (a) Left: Schematic figure of the layered structure including both electrodes and the thin film. Right: 3D sketch of capacitors with different dimensions on the film (b) Left: Layered structure for interdigitated electrode (IDE) geometry. Right: Isometric and cross sectional view of the electrode geometry, based on [33]. IDE dimensions are d=8 µm, a=8 µm and L=500 µm

Out-of-Plane - Parallel Plate Geometry

The general device structure of a capacitor is illustrated in **Figure 13a**. It consists of a substrate, bottom and top electrode, and the measured material. These are easy to fabricate because they do not require a high degree of sample uniformity and the geometry is relatively simple [34]. For my project, I used a pattern with 12.5 µm, 25 µm, 50 µm and 100 µm capacitors.

In-Plane - Interdigitated Electrode Geometry

Due to the fact that the measurement was only focusing on the in-plane axis of the material, a different design approach was necessary. Based on literature [35, 36, 34, 37], the research group of Associate Professor Martin Lane, developed their own interdigitated electrodes (IDE) geometry.

There are 20 fingers on each side, which are 8 µm in diameter, 8 µm apart and have a 500 µm overlap, which results in 39 overlapping regions. The important dimensions of the IDE structure are shown schematically in **Figure 13b**.

3.6.2 Material Selection

After the successful growth of stable single phase, fully epitaxial and strained thin films of PVO, the next step was to investigate the integration to devices structures. Several material such as $SrVO_3$, $SrRuO_3$, $LaNiO_3$ and $LaSrCuO_4$ were considered for the bottom and top electrode. In addition, platinum (Pt) and indium tin oxide (ITO) were considered to be possible top electrodes. To find the right set of electrodes, material properties and growth conditions were taken into account.

Starting with material properties, lead (Pb) is known for being highly volatile and vanadium (V) can easily form impurity phases, especially with oxygen (O). Therefore, the deposition process was set at low temperatures and under Argon gas. Based on the high temperature during the growth process (section 3.4), it was only possible to use SVO as bottom electrode.
Materials such as $LaNiO_3$ are grown under partial pressure of oxygen, which made it more challenging to grow single phase PVO. The uniformity of the electrode surface was considered as well. Therefore, $SrRuO_3$ (grown via island formation on LAO) was not the right choice either. Furthermore, material properties such as conductivity, and optical transparency are critical for optical measurements.

In conclusion, based on past literature and experiments, I chose 2 different setups (SVO as bottom electrode and Pt or ITO as top contact) for my device fabrication.

3.7 Synthesis of PVO - Integration in Device Structures

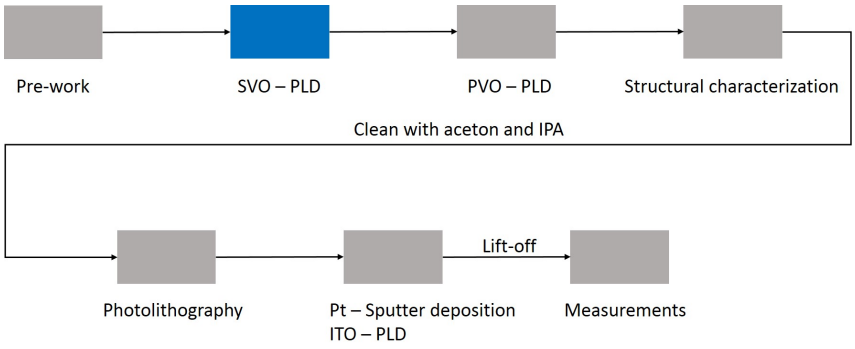

Figure 14: Fabrication process for devices from left to right. Growth of materials are done using pulsed laser and sputter deposition. Structural characterization was found by X-ray diffraction and AFM. Specific electrode geometries were produced by photolithography.

Figure 14 illustrates all fabrication steps used to get the final device. The growth conditions of SVO, PVO and ITO can be found in section 3.4, 3.3 and 3.5. Platinum was deposited on the sample using sputter deposition.

3.7.1 Parallel Plate Geometry

Based on literature [25, 28] and experience, I decided to grow a thin SVO layer (∼10 nm) as the bottom electrode, followed by a thin film of PVO (∼150 nm) using pulsed laser deposition. After structural characterization using X-ray defraction and AFM, a pattern (circular capacitors) was created by photolithography. For electrical and dielectric measurements, a platinum film (∼50 nm) was deposited as the top contact by sputtering, whereas optical measurements required a conductive and transparent top electrode. Thus, an ITO layer (∼100 nm) was grown using the same PLD system.

Substrate (LAO)/Bottom electrode (SVO)/ Thin film (PVO)/Top electrode (Pt)

X-ray diffraction and AFM results are shown in **Figure 15a**. $2\Theta/\Theta$-scan shows a highly crystalline sample of SVO (∼10 nm) and PVO (∼150 nm). The SVO layer (bottom electrode) serves as buffer between the substrate LAO(001) and the PVO film. The smoothing effect can be seen in the AFM picture (**Figure 15b**) and is verified by a RMS roughness on the order of ∼7 nm. After completion of the structural characterization, photolithography was used to pattern the sample (Figure 14). Subsequently, platinum (Pt) or indium tin oxide (ITO) was deposited as top electrode.

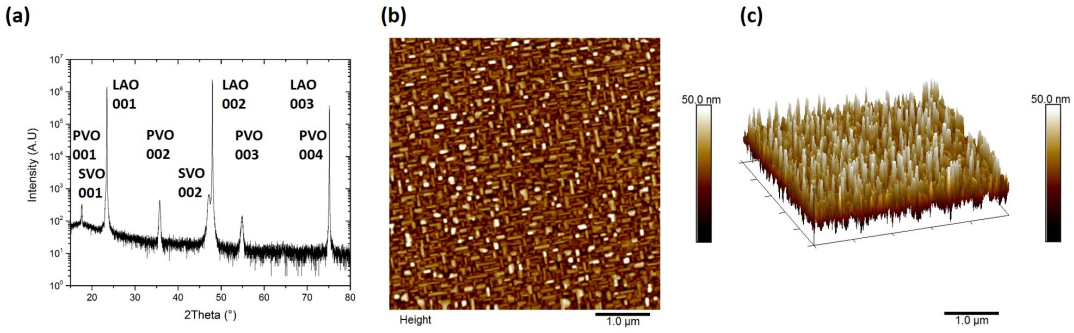

Figure 15: Structural characterization: (a) $2\Theta/\Theta$-scan of the sample. (b) AFM results showing a smoother and flatter surface morphology than a PVO single layer (Figure 9). The RMS roughness is about $\sim$7 nm.

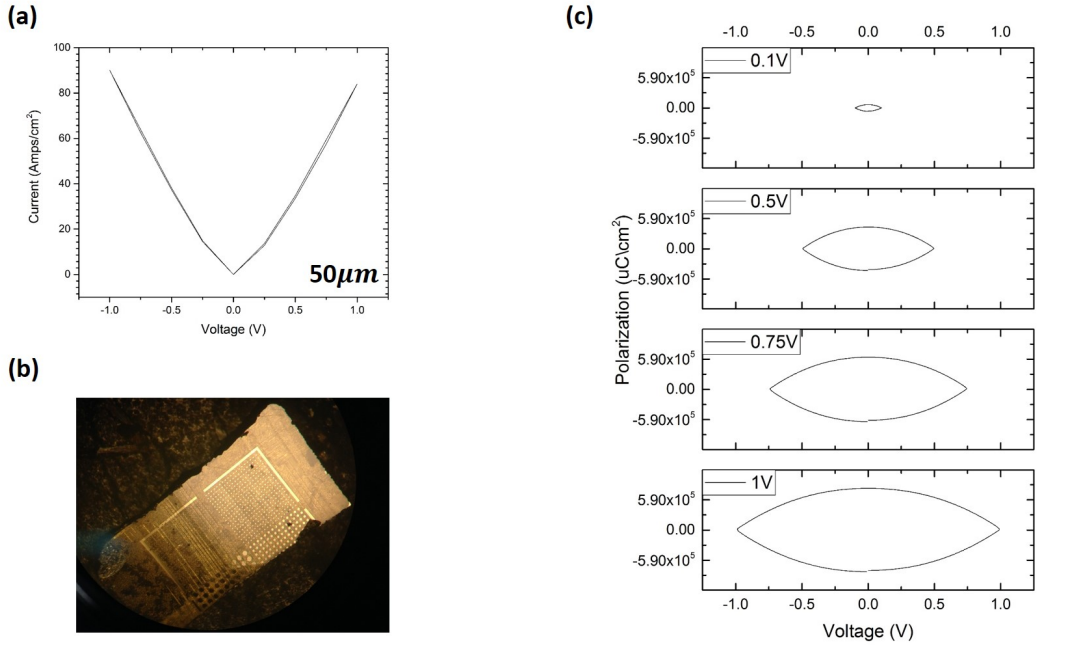

Figure 16: (a) Observed I-V curve (50 μ-capacitor) with Pt as top contact. It clearly shows ohmic behavior. All I-V curves taken are showing the same ohmic behavior, only the value of measured current changed depending on the dimension of the capacitor. (b) Final device showing the pattern of capacitors with different dimensions. (c) P-E hysteresis loops are not observable

After completion of the device fabrication process, all samples were taken to the probe station. By measuring the capacitance and the resistance (R), the resistivity (ρ), which depends on impurities, was calculated based on the dimensions of the device. R represents the resistance, A equals the area of the circular capacitor and l is the thickness of the PVO film. All PVO films exhibit resistivities between 60 to 5500 Ω cm at room temperature, which is comparable to the literature [23, 20, 19].

$$\rho = \frac{R \cdot A}{l} \tag{3.1}$$

In addition, I-V curves were taken to reveal the electronic behavior of PVO films. Results are shown in **Figure 16a**, which represent all films measured. Due to the intrinsic structure and high leakage, we only received I-V curves in ohmic shape (**Figure 16a**).

Polarization - electric field (P-E) measurements were not successful. Note that the observation of P-E loops for the isotopic $PbTiO_3$ is possible only for samples with a resistivity above $1 \times 10^{11}\,\Omega$ cm [38]. The maximum resistivity achieved in the PVO films was $\sim$5500 Ω cm. The low resistivity and intrinsic structure (high tetragonal distortion) of the PVO material prevented the observation of P-E hysteresis loop (**Figure 16c**).
Figure 16b is a photo taken during the experiment, which shows the device structure including the different dimensions of the capacitors.

Substrate (LAO)/Bottom electrode (SVO)/ Thin film (PVO)/Top electrode (ITO)

By using ITO as the top electrode, dark and light photo current measurements were possible using the probe station. The results are displayed in **Figure 17**. There was almost no difference in measuring the photo current under dark or light conditions (**Figure 17a-c**).
Only one capacitor showed a significant response to the external illumination (**Figure 17d**), but it was not reproducible on different capacitors.

Therefore, **Figure 17d** was considered as an statistical outlier produced by either a damaged probe tip or imperfect sample contact. **Figure 18** shows the pattern of capacitors, including one micromanipulator that is in contact with the ITO top electrode. The other probe tip is in contact with the bottom electrode (not in the picture).

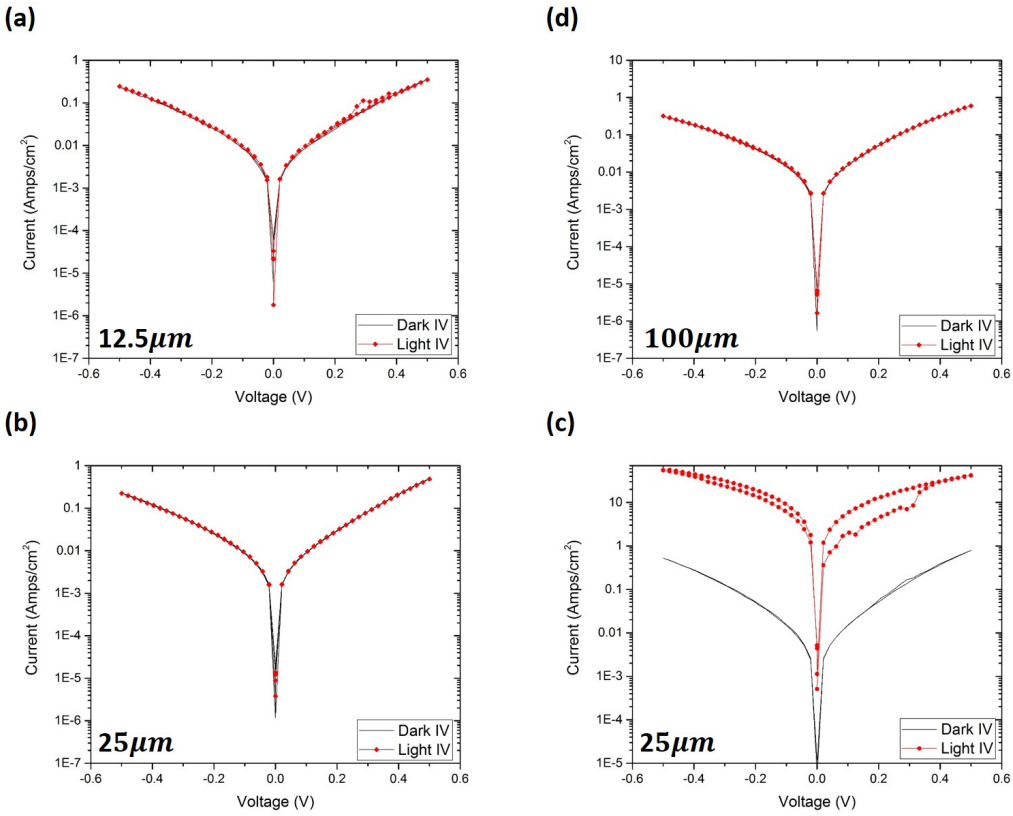

Figure 17: I-V curves of samples with ITO as top electrode. (a)-(d) show the result of I-V measurements under dark and light conditions regarding capacitors of 12.5 µm, 25 µm, 50 µm and 100 µm. Only in (c) a significant difference in current can be identified.

(a) (b)

Figure 18: Pattern of capacitors (12.5 µm, 25 µm, 50 µm and 100 µm). (a) Probe tip is in contact with one of the capacitors. Here, platinum (Pt) was used as the top electrode. The other probe tip is in contact with the bottom electrode (not in the picture). (b) ITO was deposit on the film in order to enable optical measurements.

3.7.2 Interdigitated Electrode Geometry

In contrast to the parallel plate geometry (3.7.1), the SVO deposition of the bottom electrode (blue box in **Figure 14**) was not necessary because of the planar IDE geometry. The layered structure consists of a PVO thin film (∼200 nm) followed by the top electrode, which was made out of platinum (Pt) (∼50 nm).

Substrate (LAO)/Thin film (PVO)/Top electrode (Pt)

In order to probe the thin film in the in-plane direction, IDE geometry was used. The structural characterization of PVO on LAO (001) was already shown in section 3.3, because a SVO layer was not needed as a bottom electrode.

I-V curves taken by the probe station are displayed in **Figure 19a**. The outcome was relatively similar to the results of the out-of-plane measurements. The I-V curve revealed ohmic behavior in the in-plane as well, but the current density was extremely small. As mentioned above, all results reported in this work are representative of all samples. **Figure 19b** illustrates the planar geometry of the so-called interdigitated electrode.

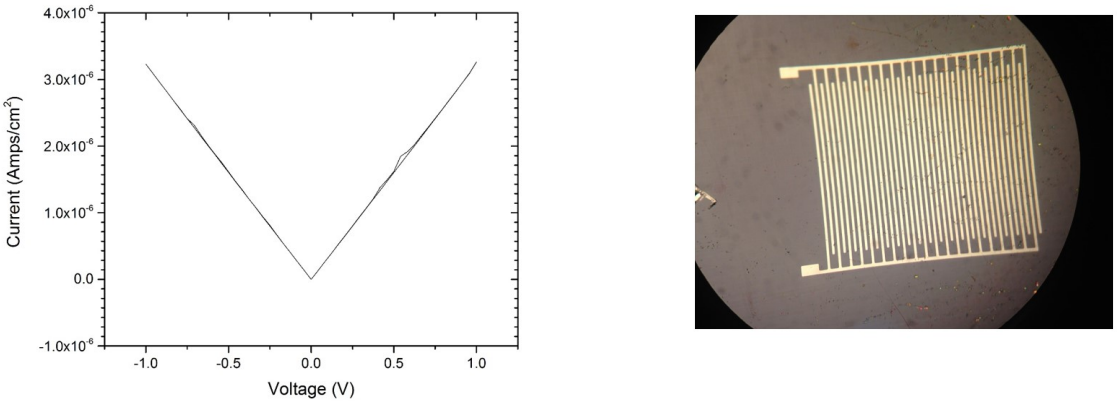

(a) (b)

Figure 19: (a) I-V curve of the IDE of PVO on LAO (001). (b) Picture taken by a light microscope, which shows the schematic geometry of the interdigitated electrode.

Initially, it was not expected to obtain ohmic behavior in all devices, irrespective the type of measurement (in-plane or out-of-plane) and electrode material (Pt or ITO). A possible explanation could be the different work functions Φ of materials and the change in band structure due to contact between different materials.

Based on literature (theoretical and experimental results), we know the work function for ITO ($\Phi_{ITO} \approx 6\ eV$), SVO ($\Phi_{SVO} \approx 4.5\ eV$) and Pt($\Phi_{Pt} \approx 5.65\ eV$) [39, 40, 41]. There are similarities between the AVO_3 perovskite structures and band structures. By taking the electron affinity of SVO ($X_{SVO} \approx= 5.5\ eV$) and the relieved energy gap of PVO ($E_g = 1.3\ eV$) [5], the estimated work function is about $\Phi_{PVO} = 6.8\ eV$.

Therefore a *schottky junction* would be present if $\Phi_s < \Phi_m$ is true , otherwise the junction would show *ohmic* behavior for $\Phi_s > \Phi_m$, where subscripts indicate semiconductor (s) and metal (m). This means, that we should receive ohmic junction on both interfaces due to the high work-function of PVO Φ_{PVO} regardless of the top electrode. Combined with the intrinsic properties (highly leaky) and unique structure of the material, this may be one possible explanation for the observed results.

4 Outlook

Presently, my supervisor **Associate Professor Martin Lane** and I are working on the final part of data analysis. The structural characterization concerning X-ray diffraction and AFM is finished. All probe station results are plotted and evaluated. However, the main focus is still on the interpretation of the ohmic behavior during the I-V measurements. We are still trying to improve our concept based on different work functions and the shift of the band structure in order to give a plausible explanation for this ohmic behavior.

Furthermore, we are evaluating the result of the ellipsometry measurements. The goal is to get insight in optical properties of PVO.

The main task of this project is the completion of the paper (to be submitted for publication in a peer-reviewed journal). Therefore I am in consultation with my supervisor in oder to write this manuscript.

5 Summary

My project was to synthesize $PbVO_3$ and subsequently characterize its structure and properties. This report started with a schematic overview of the most common investigation and characterization methods, followed by a brief historical summary of the latest results regarding materials (PVO, SVO) and the substrate LAO. In addition, pulsed laser deposition (PLD) was introduced as a thin film growth technique.

The growth of (00l) oriented single phase, highly crystalline, fully epitaxial and strained PVO thin films on LAO (001) using PLD was successful. SVO thin films were grown on LAO (001) in order to obtain a possible bottom electrode for the device fabrication process. For the top electrode I focused on platinum (Pt) and indium tin oxide (ITO) growth techniques.

Structural, chemical, electrical and dielectric properties of this highly distorted perovskite material have been investigated in depth. Additionally, optical properties were studied using ellipsometry. My supervisor and I are currently working on the final part of the data analysis. Therefore, not all results are shown in the experimental section.

6 Appendix

6.1 PLD - Thin Film Growth Technique

For many years, research of complex oxides was reserved for bulk single crystal and powder samples. Pulsed laser deposition was first discovered by Dijkkamp et. al on high T_c superconductors thin films in the late 1980's [42]. The continual improvement of the PLD procedure revolutionized complex oxide material research [43].

PLD is a simple growth technique used to synthesize high quality thin films on substrates. A typical PLD system consists of an ultra high vacuum (UHV) chamber, target holder, rotator and substrate heater (**Figure 20**). Additionally, pressure gauges, controllers and instruments to adjust and control the deposition environment were attached to the chamber [23].

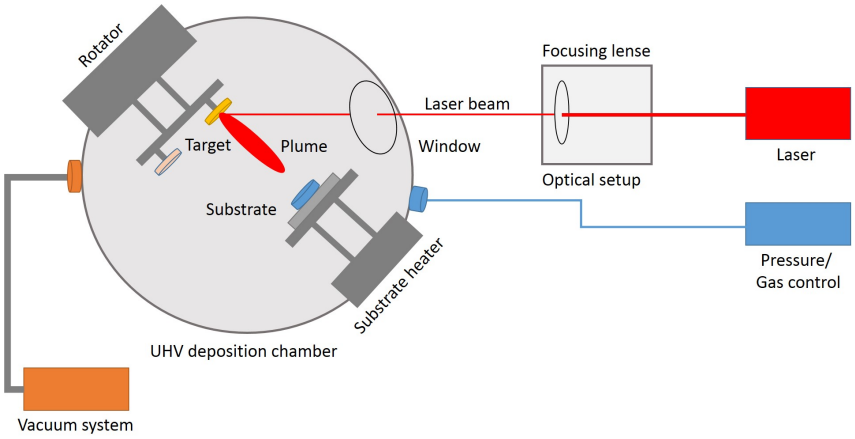

Figure 20: Schematic illustration of a typical pulsed laser chamber, including essential control elements and tools that were used to adjust the deposition environment.

The actual deposition of thin film on the substrate was achieved by the vaporization of materials by an external laser. Using a set of optics including apertures, attenuators, mirrors and lenses, the laser beam was focused into the chamber with the correct laser fluence. PLD is a non equilibrium process, which enables a stoichiometric transfer between the target and substrate [43]. The most significant advantage of PLD over other thin film processes, is that many experimental parameters such as temperature, pressure etc. can be adjusted.

Control of deposition parameters (substrate temperature, target to substrate distance, gas environment [UHV or inert gas]), and laser parameters (laser fluence, wavelength, repetition rate and pulse duration) enables a wide range of thermodynamic growth conditions. Therefore, it is possible to tune thin film properties and adjust texture, stress or interface roughness [44, 43]. Thus, PLD is a very versatile and powerful thin film technique. However, the formation of large particles or marcoparticle ejection is a well known disadvantage of pulsed laser deposition [23, 45].

6.2 Epitaxial Growth of Thin Films

This has been one of the most crucial developments in the field of semiconductor technology in the past few decades [23, 46]. Epitaxy describes the growth of a single crystal thin film on top of crystalline substrate. Based on the combination of materials, there are two major types of epitaxy, *homoepitaxy* and *heteroepitaxy*, which are illustrated in **Figure 21**.

Homoepitaxy

Refers to thin film growth of a material on a substrate of that same material. A common example is doped-Si on a Si substrate. Homoepitaxy achieves a higher quality film while avoiding defects. Furthermore, thin films can be doped independently of the substrate [46]

Heteroepitaxy

Substrate and film are different materials, but have a similar structure. Depending on the mismatch of the lattice parameters, strained or relaxed heteroepitaxy film growth occurs. The control of strain in case of a slight mismatch has a significant influence on the material's properties.

For homoepitaxy, film and substrate material are identical, lattice matched interfaces can be achieved (**Figure 21a**). This leads to a very high quality film and limited disruption (interfacial-bond straining) of the structure at the interface [46]. Due to the unmatched lattice parameters in heteroepitaxy, three different interfaces can be distinguised.
For only a slight lattice mismatch, the interfacial structure is comparable with homoepitaxy lattice match. **Figure 21b** shows strained-layer epitaxy. This interfacial structure is very common during the early film growth stages irrespective of mismatch in lattice parameter for materials with the same crystal structure (perovskite on perovskite).

For even bigger mismatches, the adaptation of their crystallographic differences is not possible. Dislocation defects are generated at the interface, to accommodate the interfacial strain leading to relaxed films [46, 23]. Hence, the previously strained material relaxes to its bulk structure (**Figure 21c**).

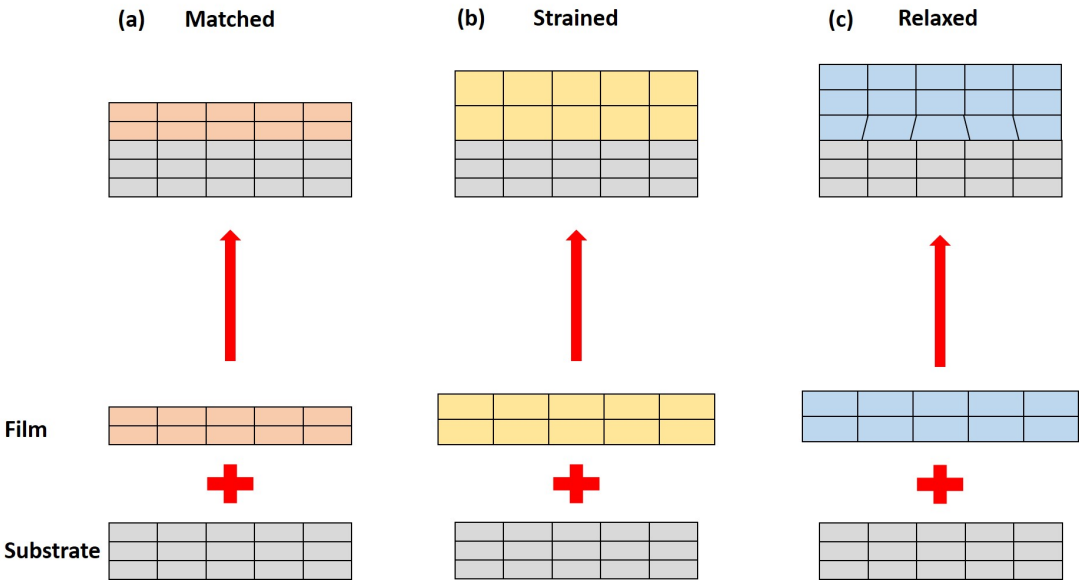

Figure 21: Illustration of three types of heteroepitaxal interfaces. (a) almost perfectly lattice matched, (b) strained and (c) relaxed heteroepitaxial structures. The schematic arrangement was adopted and modified from literature [46].

6.3 Calculation of *C*-Lattice Parameter of PVO

Phi-scans of fully epitaxial and strained thin films of PVO on LAO (001) revealed the a-lattice parameter to be 3.79 Å. Reciprocal space maps confirmed the high tetragonal distortion and the fully strained film. Thereafter, the out-of-lattice parameter c was determined to be 5.02 Å.

2Θ/Θ-scans enable a different approach to evaluate the out-of-lattice parameter c. Using the angle 2Θ, d-spacing for tetragonal systems and **Bragg equation 6.1**, the c-parameter was calculated and compared to the bulk value.

$$n\lambda = 2d_{hkl}sin(\frac{2\Theta}{2}) \tag{6.1}$$

with

$$d_{hkl} = \sqrt{\frac{a^2}{h^2+k^2} + \frac{c^2}{l^2}} \tag{6.2}$$

The corresponding c-lattice parameter was calculated to be 5.02 Å, which agrees with the RSM result and literature.
PVO bulk lattice parameters can be found in section 3.1.

6.4 Calculation of The Thickness of SVO

XRR is a very powerful measurement to obtain information about layer thickness, density and roughness of thin-layered samples [47]. The fitting and the results of the XRR-measurement were evaluated using the software *Reflectivity by PANanalytical*.

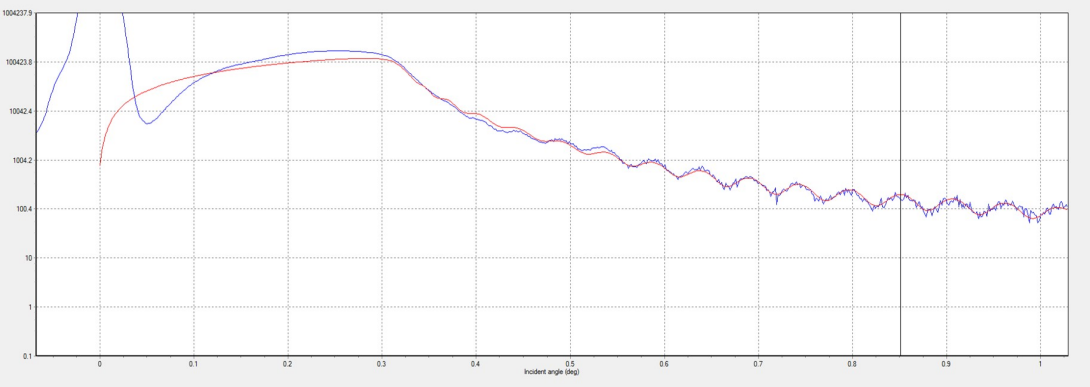

Figure 22: Plot of measurement results (blue line) and the fitting curve (red line). The so-called *Kiessing fringes* manifest itself as interference oscillations as a consequence of the angular-dependent phase shift.

Table 4 shows the fitting parameter for **Figure 10b**. **Figure 22** compares the XRR-measurement results and fitting results. The blue line indicates the experimental measurement while the red line considers fitting parameters such as thickness, density, and roughness. An average thickness of the SVO layer was determined to be 74 nm using several interference oscillations (*Kiessing fringes* [48]). Based on the calculated thickness, a growthrate of 9.42 sec per unit cell of SVO was revealed.

Table 4: Sample fitting parameters - SVO

Layer	Layer description	Density (g/cm^3)	Thickness (nm)	Roughness (nm)
3	$SrVO_3$	8.49	0.89	1.47
2	$SrVO_3$	5.32	72.91	0.57
1	$SrVO_3$	6.61	0.26	2.66
Substrate	$LaAlO_3$	6.24	600000	0.49

6.5 Photolithography

Photolithography is a method used to pattern a thin film or bulk of a material. The geometric pattern from a photomask was transferred to a light-sensitive photoresist (PR) on the substrate using UV light. Etch or lift off process enabled the removal of the remaining PR with the target material on its surface. **Figure 23** shows the basic procedure used for all my devices in more detail.

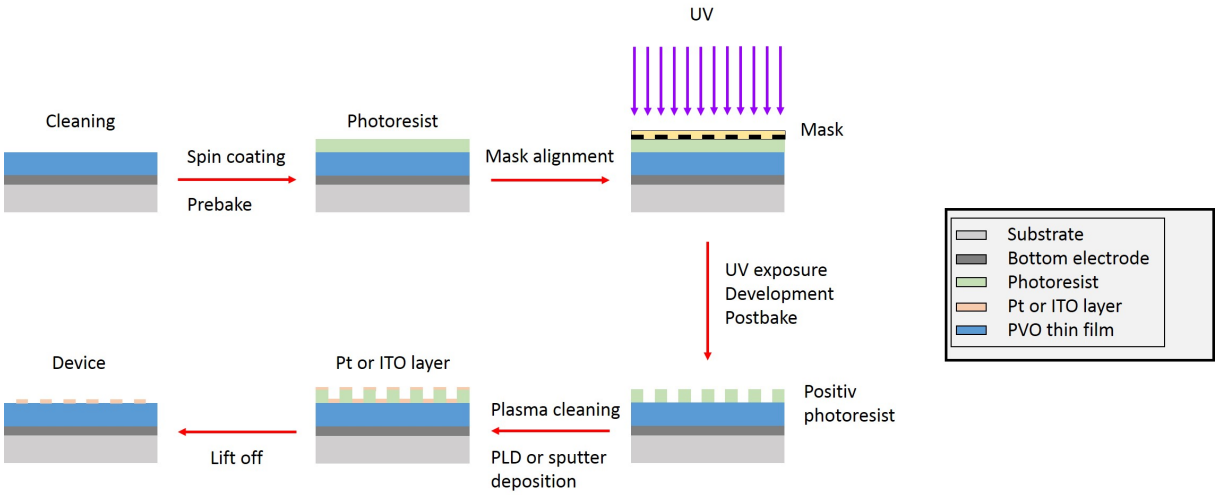

Figure 23: Schematic illustration of all steps during a photolithography process in microfabrication. Photolithography starts with the cleaning process of the sample, followed by the photoresist application. Exposure and development represent the essential part of photolithography. The final step considers the deposition of the top contact and subsequent lift-off process.

Cleaning

To ensure high quality pattern on the substrate without any contaminations, all films were ultrasonicated for about 3 minutes each in acetone and the IPA.

Photoresist Application

A positive photoresist by *G-line* (the exposed part of the PR to UV becomes soluble to the PR developer) was deposited on the sample using a spin coater, which created a uniform layer of the photoresist. The spin coater started at 1000 rpm for 10 seconds followed by 6000 rpm for another 30 seconds. The samples were placed on a heater at 95 °C for 3 minutes (*prebaked*).

Exposure to UV Light and Development

A mask with a specific pattern was placed on top of the sample. The positive photoresist was exposed to a pattern of UV light. Due to a chemical reaction, the exposed part became

soluble to the developer, whereas the unexposed part remained insoluble. The capacitor pattern (12.5 µm, 25 µm, 50 µm and 100 µm) and IDE geometry were used. The soluble PR was removed by washing the sample with a 3:1 solution of DI-water and *AZ-400k developer*. All samples were *hard baked* at 110 °C for 15 minutes to increase the durability for the subsequent deposition.

Deposition of the Top Contact and Lift-Off Process

In order to maintain a high quality pattern, all samples were plasma cleaned at 800 mtorr in O_2 for 2 minutes. After the deposition of platinum (Pt) or indium tin oxide (ITO) as the top contact, the lift-off process was the finale procedure. The remaining PR along with the the top layer on its surface was removed with acetone. Thus, the target material (Pt or ITO) remained only in the regions that were in direct contact with the film. The quality of the pattern was controlled using light microscopy.

7 Bibliography

[1] R. Ramesh and N. A. Spaldin. "Multiferroics: progress and prospects in thin films". *Nature materials* 6 (1) (2007), pp. 21–29 (cit. on p. 2).

[2] L. W. Martin et al. "Growth and structure of PbVO3 thin films". *Applied physics letters* 90 (6) (2007), p. 062903 (cit. on pp. 2, 6, 7, 10).

[3] S.-W. Cheong and M. Mostovoy. "Multiferroics: a magnetic twist for ferroelectricity". *Nature materials* 6 (1) (2007), pp. 13–20 (cit. on p. 2).

[4] N. A. Hill. "Why Are There so Few Magnetic Ferroelectrics?" *The Journal of Physical Chemistry B* 104 (29) (2000), pp. 6694–6709 (cit. on p. 2).

[5] A. Kumar et al. "Linear and nonlinear optical properties of multifunctional PbVO3 thin films". *Applied Physics Letters* 92 (23) (2008) (cit. on pp. 2, 22).

[6] W. Zhou et al. "Structural properties of PbVO 3 perovskites under hydrostatic pressure conditions up to 10.6 GPa". *Journal of Physics: Condensed Matter* 24 (43) (2012), p. 435403 (cit. on pp. 2, 6, 7).

[7] K Inaba. "X-Ray Thin-Film Measurement Techniques I. Overview". *The Rigaku Journal* 24 (1) (2008), pp. 10–15 (cit. on pp. 2, 3).

[8] T Mitsunaga. "X-Ray Thin-Film Measurement Techniques II. Out-of-plane diffraction measurements". *The Rigaku Journal* 25 (1) (2009), pp. 7–12 (cit. on p. 2).

[9] PANalytical. *X'PERT3 Family: preFIX hybrid monochromators*. 2015 (cit. on p. 2).

[10] V. L. Mironov. *Fundamentals of scanning probe microscopy*. 2004, p. 144 (cit. on p. 3).

[11] E. Meyer, H. J. Hug, and R. Bennewitz. *Scanning probe microscopy: the lab on a tip*. Springer Science & Business Media, 2013 (cit. on p. 4).

[12] R. Wiesendanger. *Scanning probe microscopy and spectroscopy: methods and applications*. Cambridge University Press, 1994 (cit. on p. 4).

[13] W. Heywang, K. Lubitz, and W. Wersing. *Piezoelectricity: evolution and future of a technology*. Vol. 114. Springer Science & Business Media, 2008 (cit. on p. 4).

[14] J. I. AG. *Piezoresponse force microscopy*. 2014 (cit. on p. 4).

[15] R. Waser. *Nanoelectronics and information technology*. John Wiley & Sons, 2012 (cit. on p. 4).

[16] M. Johnsson and P. Lemmens. "Crystallography and chemistry of perovskites". *Handbook of magnetism and advanced magnetic materials* (2007) (cit. on p. 6).

[17] N. A. Hill and A. Filippetti. "Why are there any magnetic ferroelectrics?" *Journal of Magnetism and Magnetic Materials* 242 (2002), pp. 976–979 (cit. on p. 6).

[18] J. Wang et al. "Epitaxial BiFeO3 multiferroic thin film heterostructures". *Science* 299 (5613) (2003), pp. 1719–1722 (cit. on p. 6).

[19] R. V. Shpanchenko et al. "Synthesis, structure, and properties of new perovskite PbVO3". *Chemistry of materials* 16 (17) (2004), pp. 3267–3273 (cit. on pp. 6, 7, 19).

[20] A. A. Belik et al. "Crystallographic features and tetragonal phase stability of PbVO3, a new member of PbTiO3 family". *Chemistry of materials* 17 (2) (2005), pp. 269–273 (cit. on pp. 6–8, 19).

[21] Y. Uratani et al. "First-principles predictions of giant electric polarization". *Japanese journal of applied physics* 44 (9S) (2005), p. 7130 (cit. on p. 7).

[22] K. Oka et al. "Magnetic ground-state of perovskite PbVO3 with large tetragonal distortion". *Inorganic chemistry* 47 (16) (2008), pp. 7355–7359 (cit. on p. 7).

[23] L. W. Martin. "Engineering multiferroic materials and new functionalities in materials". PhD thesis. 2008 (cit. on pp. 7, 19, 25, 26).

[24] A. Kumar et al. "Polar and magnetic properties of Pb V O 3 thin films". *Physical Review B* 75 (6) (2007), p. 060101 (cit. on p. 7).

[25] Y. Lan, X. Chen, and M He. "Structure, magnetic susceptibility and resistivity properties of SrVO 3". *Journal of alloys and compounds* 354 (1) (2003), pp. 95–98 (cit. on pp. 8, 9, 17).

[26] S.-y. Yan et al. "Electronic structures and ferroelectric instabilities of cubic AV O3 (A= Sr, Ba, and Pb) perovskites by first-principles calculations". *Journal of Physics: Condensed Matter* 22 (12) (2010), p. 125501 (cit. on p. 8).

[27] H. B. Alipour. "Atomic Structure and Chemistry of Defects in SrVO3 Thin Films". MA thesis. 2013 (cit. on p. 8).

[28] J. A. Moyer, C. Eaton, and R. Engel-Herbert. "Highly Conductive SrVO3 as a Bottom Electrode for Functional Perovskite Oxides". *Advanced Materials* 25 (26) (2013), pp. 3578–3582 (cit. on pp. 9, 17).

[29] M Ishii et al. "Improvement of organic electroluminescent device performance by in situ plasma treatment of indium–tin-oxide surface". *Journal of Luminescence* 87 (2000), pp. 1165–1167 (cit. on p. 14).

[30] J. Dai et al. "Organic photovoltaic cells with near infrared absorption spectrum". *Applied Physics Letters* 91 (25) (2007), p. 3503 (cit. on p. 14).

[31] C.-Y. Ho et al. "Investigation of post-annealing indium tin oxide for future electro-optical device application". *Proceedings of the 10th WSEAS international conference on Telecommunications and informatics and microelectronics, nanoelectronics, optoelectronics, and WSEAS international conference on Signal processing*. World Scientific, Engineering Academy, and Society (WSEAS). 2011, pp. 154–158 (cit. on p. 14).

[32] M. Girtan et al. "Influence of oxidation conditions on the properties of indium oxide thin films". *Applied surface science* 162 (2000), pp. 492–498 (cit. on p. 14).

[33] N. Kidner et al. "Modeling interdigital electrode structures for the dielectric characterization of electroceramic thin films". *Thin solid films* 496 (2) (2006), pp. 539–545 (cit. on p. 15).

[34] C. M. Folkman. "Spontaneous strain and ferroelectric-ferroelastic behavior in epitaxial bismuth ferrite thin films". PhD thesis. 2010 (cit. on p. 15).

[35] G. W. Farnell et al. *Capacitance and field distributions for interdigital surface-wave transducers*. Tech. rep. DTIC Document, 1969 (cit. on p. 15).

[36] O. Vendik, S. Zubko, and M. Nikol'skii. "Modeling and calculation of the capacitance of a planar capacitor containing a ferroelectric thin film". *Technical Physics* 44 (4) (1999), pp. 349–355 (cit. on p. 15).

[37] S. S. Gevorgian et al. "CAD models for multilayered substrate interdigital capacitors". *Microwave Theory and Techniques, IEEE Transactions on* 44 (6) (1996), pp. 896–904 (cit. on p. 15).

[38] R. Nelmes and W. Kuhs. "The crystal structure of tetragonal PbTiO 3 at room temperature and at 700 K". *Solid state communications* 54 (8) (1985), pp. 721–723 (cit. on p. 19).

[39] Y Park et al. "Work function of indium tin oxide transparent conductor measured by photoelectron spectroscopy". *Applied Physics Letters* 68 (19) (1996), pp. 2699–2701 (cit. on p. 22).

[40] M Takizawa et al. "Coherent and incoherent d band dispersions in SrVO 3". *Physical Review B* 80 (23) (2009), p. 235104 (cit. on p. 22).

[41] D. R. Lide. *CRC handbook of chemistry and physics*. CRC press, 2004, pp. 12–114 (cit. on p. 22).

[42] D Dijkkamp et al. "Preparation of Y-Ba-Cu oxide superconductor thin films using pulsed laser evaporation from high Tc bulk material". *Applied Physics Letters* 51 (8) (1987), pp. 619–621 (cit. on p. 25).

[43] D. B. Chrisey and G. K. Hubler. "Pulsed laser deposition of thin films" (1994) (cit. on pp. 25, 26).

[44] T Scharf and H. Krebs. "Influence of inert gas pressure on deposition rate during pulsed laser deposition". *Applied Physics A* 75 (5) (2002), pp. 551–554 (cit. on p. 26).

[45] H.-U. Krebs et al. "Pulsed Laser Deposition (PLD)–A Versatile Thin Film Technique". *Advances in Solid State Physics*. Springer, 2003, pp. 505–518 (cit. on p. 26).

[46] M. Ohring. *Materials science of thin films*. Academic press, 2001 (cit. on pp. 26, 27).

[47] M. Yasaka. "X-Ray Thin-Film Measurement Techniques V. X-ray reflectivity measurement". *The Rigaku Journal* 26 (2) (2010), pp. 1–9 (cit. on p. 28).

[48] H Kiessig. "Investigations into the total reflexion of roetgen rays". *Annalen der Physik* 10 (6) (1931), pp. 715–768 (cit. on p. 28).